Research Article | Vol. 25, No. 5 | 6 Mar 2017 | OPTICS EXPRESS 5327

Optics EXPRESS

Optical properties of $Cu_2ZnSnSe_4$ thin films and identification of secondary phases by spectroscopic ellipsometry

ÖZDEN DEMIRCIOĞLU,[1] JOSÉ FABIO LÓPEZ SALAS,[1] GERMAIN REY,[2] THOMAS WEISS,[2,3] MARINA MOUSEL,[2] ALEX REDINGER,[2,4] SUSANNE SIEBENTRITT,[2] JÜRGEN PARISI,[1] AND LEVENT GÜTAY[1*]

[1]*Laboratory for Chalcogenide Photovoltaics, Department of Energy and Semiconductor Research, Institute of Physics, University of Oldenburg, D-26111 Oldenburg, Germany;*
[2]*Laboratory for Photovoltaics, University of Luxembourg, Belvaux, Luxembourg*
[3]*Current address: Laboratory for Thin Films and Photovoltaics, Empa, Swiss Federal Laboratories for Materials Science and Technology, 8600 Dübendorf, Switzerland.*
[4]*Current address: Helmholtz Zentrum Berlin, Department Complex Compound Semiconductor Materials for Photovoltaics, 14109 Berlin, Germany*
**levent.guetay@uni.oldenburg.de*

Abstract: We apply spectroscopic ellipsometry (SE) to identify secondary phases in $Cu_2ZnSnSe_4$ (CZTSe) absorbers and to investigate the optical properties of CZTSe. A detailed optical model is used to extract the optical parameters, such as refractive index and extinction coefficient in order to extrapolate the band gap values of CZTSe samples, and to obtain information about the presence of secondary phases at the front and back sides of the samples. We show that SE can be used as a non-destructive method for detection of the secondary phases ZnSe and $MoSe_2$ and to extrapolate the band gap values of CZTSe phase.

OCIS codes: (310.0310) Thin films; (310.6860) Thin films, optical properties.

References and links

1. I. Repins, C. Beall, N. Vora, C. DeHart, D. Kuciauskas, P. Dippo, B. To, J. Mann, W. C. Hsu, A. Goodrich, and R. Noufi, "Co-evaporated Cu2ZnSnSe4 films and devices," Sol. Energy Mater. Sol. Cells **101**, 154–159 (2012).
2. C. Wadia, A. P. Alivisatos, and D. M. Kammen, "Materials availability expands the opportunity for large-scale photovoltaics deployment," Environ. Sci. Technol. **43**(6), 2072–2077 (2009).
3. K. Ito and T. Nazakawa, "Electrical and optical properties of stannite-type quaternary semiconductor thin films," Jpn. J. Appl. Phys. **27**, 2094 (1988).
4. H. Katagiri, K. Saitoh, T. Washio, H. Shinohara, T. Kurumadani, and S. Miyajima, "Development of thin solar cell based on Cu2znSnS4 thin films," Sol. Energy Mater. Sol. Cells **65**(1-4), 141–148 (2001).
5. C. Persson, "Electronic and optical properties of Cu2ZnSnS4 and Cu2ZnSnSe4," J. Appl. Phys. **107**(5), 053710 (2010).
6. S. Siebentritt and S. Schorr, "Kesterites–a challenging material for solar cells," Prog. Photovolt. Res. Appl. **20**(5), 512–519 (2012).
7. W. Wang, M. T. Winkler, O. Gunawan, T. Gokmen, T. K. Todorov, Y. Zhu, and D. B. Mitzi, "Device characteristics of CZTSSe thin-film solar cells with 12.6% efficiency," Adv. Energy Mater. **4**(7), 1301465 (2014).
8. Y. S. Lee, T. Gershon, O. Gunawan, T. K. Todorov, T. Gokmen, Y. Virgus, and S. Guha, "Cu2ZnSnSe4 thin-film solar cells by thermal co-evaporation with 11.6% efficiency and improved minority carrier diffusion length," Adv. Energy Mater. **5**(7), 1401372 (2015).
9. J. Kim, H. Hiroi, T. K. Todorov, O. Gunawan, M. Kuwahara, T. Gokmen, D. Nair, M. Hopstaken, B. Shin, Y. S. Lee, W. Wang, H. Sugimoto, and D. B. Mitzi, "High efficiency $Cu_2ZnSn(S,Se)_4$ solar cells by applying a double In_2S_3/CdS emitter," Adv. Mater. **26**(44), 7427–7431 (2014).
10. A. Redinger, K. Hönes, X. Fontané, V. Izquierdo-Roca, E. Saucedo, N. Valle, A. Pérez-Rodríguez, and S. Siebentritt, "Detection of a ZnSe secondary phase in coevaporated Cu2ZnSnSe4 thin films," Appl. Phys. Lett. **98**(10), 101907 (2011).
11. J. T. Watjen, J. Engman, M. Edoff, and C. Platzer-Björkman, "Direct evidence of current blocking by ZnSe in Cu2ZnSnSe4 solar cells," Appl. Phys. Lett. **100**(17), 173510 (2012).
12. H. Xie, Y. Sánchez, S. López-Marino, M. Espíndola-Rodríguez, M. Neuschitzer, D. Sylla, A. Fairbrother, V. Izquierdo-Roca, A. Pérez-Rodríguez, and E. Saucedo, "Impact of Sn(S,Se) secondary phases in Cu2ZnSn(S,Se)4

#281766 https://doi.org/10.1364/OE.25.005327
Journal © 2017 Received 30 Nov 2016; revised 25 Jan 2017; accepted 6 Feb 2017; published 28 Feb 2017

Optics EXPRESS

solar cells: a chemical route for their selective removal and absorber surface passivation," ACS Appl. Mater. Interfaces **6**(15), 12744–12751 (2014).
13. H. Fujiwara, *Spectroscopic Ellipsometry - Principles and Applications*, Wiley, 2007.
14. Ö. Demircioğlu, M. Mousel, A. Redinger, G. Rey, T. Weiss, S. Siebentritt, I. Riedel, and L. Gütay, "Detection of a MoSe2 secondary phase layer in CZTSe by spectroscopic ellipsometry," J. Appl. Phys. **118**(18), 185302 (2015).
15. J. A. Woollam Co., Inc., *Guide to Using WVASE32, Software for Spectrocopic Ellipsometry Data Acquisition and Analysis*, Chap. 8, page 8–32.
16. M. Mousel, T. Schwarz, R. Djemour, T. P. Weiss, J. Sendler, J. C. Malaquias, A. Redinger, O. Cojocaru-Mirédin, P.-P. Choi, and S. Siebentritt, "Cu-Rich Precursors Improve Kesterite Solar Cells," Adv. Energy Mater. **4**(2), 1300543 (2014).
17. A. Redinger, J. Sendler, R. Djemour, T. P. Weiss, G. Rey, P. J. Dale, and S. Siebentritt, "Different bandgaps in $Cu_2ZnSnSe_4$: Ahigh temperature coevaporation study," IEEE Photovoltaics **5**, 641–648 (2015).
18. D. E. Aspnes and A. A. Studna, "Dielectric functions and optical parameters of Si, Ge, GaP, GaAs, GaSb, InP, InAs, and InSb from 1.5 to 6.0 eV," Phys. Rev. B **27**(2), 985–1009 (1983).
19. J. J. Scragg, P. J. Dale, D. Colombara, and L. M. Peter, "Thermodynamic aspects of the synthesis of thin-film materials for solar cells," ChemPhysChem **13**(12), 3035–3046 (2012).
20. T. Schwarz, O. Cojocaru-Mirédin, P. Choi, M. Mousel, A. Redinger, S. Siebentritt, and D. Raabe, "Atom probe study of Cu2ZnSnSe4 thin-films prepared by co-evaporation and post deposition annealing," Appl. Phys. Lett. **102**(4), 042101 (2013).
21. D. A. G. Bruggeman, "Dielektrizitätskonstanten und leitfähigkeiten der mishkörper aus isotropen und anisotropen substanzen," Ann. Physik (Leipzig) **24**, 636 (1935).
22. J. C. M. Garnett, "Colours in metal glasses and in metallic films," Philos. Trans. R. Soc. London, Series A **203**, 385 (1904).
23. Y. Yu-Manuel and P. Cardona, *Fundamentals of Semiconductors Physics and Material Properties*, 4th Edition (2010).
24. L. Gütay, A. Redinger, R. Djemour, and S. Siebentritt, "Lone conduction band in $Cu_2ZnSnSe_4$," Appl. Phys. Lett. **100**(10), 102113 (2012).
25. M. León, S. Levcenko, R. Serna, I. V. Bodnar, A. Nateprov, M. Guc, G. Gurieva, N. Lopez, J. M. Merino, R. Caballero, S. Schorr, A. Perez-Rodriguez, and E. Arushanov, "Spectroscopic ellipsometry study of $Cu_2ZnSnSe_4$ bulk crystals," Appl. Phys. Lett. **105**(6), 061909 (2014).
26. G. Zoppi, I. Forbes, R. W. Miles, P. J. Dale, J. J. Scragg, and L. M. Peter, "$Cu_2ZnSnSe_4$ thin film solar cells produced by selenisation of magnetron sputtered precursors," Prog. Photovolt. Res. Appl. **17**(5), 315–319 (2009).
27. S. Chen, X. G. Gong, A. Walsh, and S.-H. Wei, "Crystal and electronic band structure of Cu2ZnSnX4 (X= S and Se) photovoltaic absorbers: First-principles insights," Appl. Phys. Lett. **94**(4), 041903 (2009).
28. G. Rey, A. Redinger, J. Sendler, T. P. Weiss, M. Thevenin, M. Guennou, B. El Adib, and S. Siebentritt, "The band gap of Cu2ZnSnSe4: Effect of order-disorder," Appl. Phys. Lett. **105**(11), 112106 (2014).
29. S. Ahn, S. Jung, J. Gwak, A. Cho, K. Shin, K. Yoon, D. Park, H. Cheong, and J. H. Yun, "Determination of band gap energy (Eg) of Cu2ZnSnSe4 thin films: On the discrepancies of reported band gap values," Appl. Phys. Lett. **97**(2), 021905 (2010).
30. R. Djemour, M. Mousel, A. Redinger, L. Gütay, A. Crossay, D. Colombra, P. J. Dale, and S. Siebentritt, "Detecting ZnSe secondary phase in Cu2ZnSnSe4 by room temperature photoluminescence," Appl. Phys. Lett. **102**(22), 222108 (2013).
31. S. Siebentritt, G. Rey, A. Finger, D. Regesch, J. Sendler, T. P. Weiss, and T. Bertram, "What is the band gap of kesterite?" Sol. Energy Mater. Sol. Cells **158**, 126–129 (2016).
32. G. Rey, T. P. Weiss, J. Sendler, A. Finger, C. Spindler, F. Werner, M. Melchiorre, M. Hála, M. Guennou, and S. Siebentritt, "Ordering kesterite improves solar cells: A low temperature post-deposition annealing study," Sol. Energy Mater. Sol. Cells **151**, 131–138 (2016).
33. R. Kondrotas, R. Juskénas, A. Naujokaitis, G. Niaura, Z. Mockus, S. Kanapeckaité, B. Cechavicius, K. Juskevicius, E. Saucedo, and Y. Sánchez, "Investigation of selenization process of electrodeposited Cu-ZnSn precursor for $Cu_2ZnSnSe_4$ thin-film solar cells," Thin Solid Films **589**, 165–172 (2015).
34. A. Redinger, D. M. Berg, P. J. Dale, R. Djemour, L. Gütay, T. Eisenbarth, N. Valle, and S. Siebentritt, "Route toward high-efficiency single phase Cu2ZnSn(S,Se)4 thin film solar cells: model experiments and literature review," IEEE J. Photovoltaics **2**(2), 200–206 (2011).
35. A. Redinger, M. Mousel, R. Djemour, L. Gütay, N. Valle, and S. Siebentritt, "$Cu_2ZnSnSe_4$ thin film solar cells produced via co-evaporation and annealing including $SnSe_2$ capping layer," Prog. Photovolt. Res. Appl. **22**(1), 51–57 (2014).
36. E. Daub and P. Würfel, "Ultralow values of the absorption coefficient of Si obtained from luminescence," Phys. Rev. Lett. **74**(6), 1020–1023 (1995).
37. L. Gütay and G. H. Bauer, "Local fluctuations of absorber properties of Cu(In,Ga)Se2 by sub-micron resolved PL towards "real life" conditions," Thin Solid Films **517**(7), 2222–2225 (2009).
38. T. Unold and L. Gütay, in: D. Abou-Ras, T. Kircharzt, U. Rau (Eds.), *Advanced Characterization Techniques for Thin Film Solar Cells*, (WILEY-VCH, 2011), Chap. 7.

Optics EXPRESS

1. Introduction

In recent years, the quaternary semiconductors $Cu_2ZnSn(S, Se)_4$ (CZTSSe) have been investigated as an alternative absorber to the current thin-film solar cell technologies. Their lower toxicity and higher earth-abundance promise low-cost production and a clean solar cell technology. With a direct band gap in the range of 1.0 eV for CZTSe and 1.5 eV for CZTS with high absorption coefficients of $>10^4$ cm^{-1} slightly above the band gap, this material family has been demonstrated to be suitable for technological application in thin film solar cell devices [1–7]. In laboratory cells, the best-reported efficiency for pure selenide based CZTSe solar cells is 11.6% [8], and for CZTSSe material, it amounts to 12.7%, a promising performance for solar cells [9]. Despite these suitable optical properties and rising interest, there are difficulties in applying this material commercially as an absorber in solar cells. One of the major obstacles is the formation of secondary phases during the growth process, which can be detrimental to the solar cell performance [6, 10–12]. Therefore, it is important to investigate CZTSSe absorbers with a quick and non-destructive method to identify structural properties and the existence of secondary phases. Hence, spectroscopic ellipsometry (SE) is favorable to make fast and non-destructive investigations. SE can be used to collect information on sample structure, the presence of secondary phases and optical properties such as complex dielectric constants, etc [13–15].

In this paper, we focus on the detection of present secondary phases at the front and back interface regions of the CZTSe thin film and the extraction of band gap values of the absorber. We demonstrate an extended optical model which includes multiple interfaces and intermixing layers, to provide a detailed analysis of the sample structure and to identify present ZnSe and $MoSe_2$ phases, which remain the most prevalent secondary phases in CZTSe absorbers even after process optimization. We obtained all analyzed specimen from solar cell relevant sample batches. Therefore, the presented method and all obtained results are relevant to fundamental investigations as well as for application in solar cell processing and process controlling.

2. Experimental details

2.1 Sample information

In this work, three $Cu_2ZnSnSe_4$ (CZTSe) thin film samples (referred to as Sample A, Sample B, and Sample C) have been investigated by using spectroscopic ellipsometry (SE), spectrophotometry(RT), Raman scattering spectroscopy and photoluminescence (PL).

Sample A and Sample B were fabricated by a high-temperature co-evaporation process, sample C was grown by a two-stage process, i.e. low-temperature co-evaporation with subsequent annealing in Se-SnSe atmosphere. All samples were fabricated at the University of Luxembourg [16,17]. The samples were deposited onto molybdenum (Mo) coated soda lime glass (SLG). The composition of sample A is Cu/(Zn + Sn) ≈0.9 and Zn/Sn≈0.94, and the composition of sample B is Cu/(Zn + Sn) ≈0.9 and Zn/Sn≈0.9. Solar cell efficiencies of companion samples give ≈6%. The composition of sample C is Cu/(Zn + Sn) ≈0.8 and Zn/Sn≈1.2, efficiencies from similar samples yield ≈5%. Sample compositions for all samples were measured by Energy Dispersive X-Ray spectroscopy (EDX). Solar cell efficiencies were measured at AM1.5-equivalent excitation.

All SE measurements were done on SLG/Mo/CZTSe samples, as one of the major scopes of this study is the detection of secondary phases at the CZTSe/Mo interface by a non-destructive technique. To confirm the SE results by further methods, i.e. Raman, PL, SEM, etc., the interface region between SLG/Mo and CZTSe was accessed by mechanical lift-off of the absorber with superglue for all samples. Thus, further measurements could be performed on the front and back sides of the absorbers and the remaining substrate surfaces to cross-check SE results.

Optics EXPRESS

Sample surfaces were etched before SE measurements to remove oxides and to reduce surface roughness for improvement of the signal-noise-ratios [18]. However, due to the differences in sample morphology and composition, it was necessary to use different etching times and etchants for each sample. Sample A and Sample B were etched with 37wt% hydrochloric acid (HCl) and, sample C was etched by 0.02 M Br_2-MeOH. For each sample, 30 sec etching time was applied before SE measurements. Further, sample A and sample B were etched by HCl before PL measurements for additional 30 sec to improve the signal quality.

2.2 Sample characterization

Spectroscopic ellipsometry (SE) was performed by using a rotating analyzer setup (J. A. Woollam Co, VASE) in the wavelength range from 240 nm to 1700 nm with a step size of 10nm at variable incidence angles (65°, 70° and 75°), on SLG/Mo/CZTSe. Optical reflection & transmission (RT) measurements were performed on lifted-off absorbers on a microscopic glass slide in the wavelength range from 800 nm to 1800 nm by using an integrating sphere. Raman scattering spectroscopy was done with 532 nm ("green" excitation) and 457.9 nm ("blue" excitation) at 3 and 1 mW excitation laser power with a spot size of ~1µm, respectively, in a LabRAM Aramis from Horiba. Photoluminescence (PL) was applied at five different excitation wavelengths (532 nm, 575 nm, 600 nm, 630 nm, and 675 nm) to differentiate between optical transitions of the absorber and present secondary phases. Laser power was kept constant at 2.4 mW with a spot size ~1.5 mm and a detection unit with an InGaAs photomultiplier and a monochromator was used. PL and Raman were measured on the front and back side of each absorber. All measurements were done at room temperature.

3. Results and Discussion

3.1 SE data analysis and optical model design

Spectroscopic ellipsometry (SE) is a non-destructive technique to analyze the optical properties of thin films. However, it is an indirect characterization method because direct conversion of measured parameters (Δ and Ψ) into optical parameters is only valid for very simple cases such as infinitely thick, homogenous and isotropic samples [13]. Therefore, the optical parameters can only be extracted from the measured data by a fitting procedure with an optical model which contains the characteristics of the sample structure, i.e. all present layers in the sample stack with thicknesses and optical functions of each material (ideally from a reference database). Unknown optical functions can be generated based on Fresnel's equation by using Herzinger-Johs Psemi oscillators [15]. Each PSemi-*M0* oscillator has seven different fit parameters: A- amplitude, E- Center Energy, B- Broadening, WR- Endpoint positions relative to center energy (E), PR- Horizontal position of the right control point relative to the center energy and endpoints, AR- Relative magnitude of the right control points, and O2R- Coefficients for the second order terms in polynomials on the right side of PSemi-*M0* oscillators, respectively. For the fitting procedure, five Psemi-*M0* oscillators were used for each sample. The fitting procedure then contains i) generation of optical functions, ii) translation of these functions via the modeling of the layer structure into theoretical Ψ and Δ, iii) comparison of these calculated values with the measured ones, and then turning back to step i) introducing changes to the oscillators until the best fit for calculated and measured Ψ- and Δ-values is found.

In our previous work, we showed that the detection of a $MoSe_2$ secondary phase layer at the back interface and the determination of its thickness are possible by data evaluation with a detailed optical model [14]. To generate a more comprehensive model of the investigated samples, we tried numerous different modeling approaches (not discussed in detail here) to introduce a reliable fitting procedure for the characterization of uniformity, crystallinity and interfacial regions and detection of further secondary phases in the sample.

Optics EXPRESS

The model design in this manuscript contains CZTSe, $MoSe_2$, ZnSe, and the Mo substrate layers. We consider $MoSe_2$ secondary phase in the model because it is easily formed at the CZTSe/Mo interface in many preparation processes due to Selenium (Se) loss to the substrate and decomposition of CZTSe at the backside and the excess Se during the preparation process. In Zn-rich conditions, ZnSe can occur in the whole layer. However, it is often found to segregate at the front or back surface, where its occurrence can be driven by decomposition reactions of the CZTSe absorber [19]. As discussed in Section 2.1, only sample C shows Zn-rich composition at the end of the process. However, SIMS profiles of the complete solar cells for sample A and sample B show Zn and Se accumulation at the back side of absorbers (not shown here). Therefore, for all three samples, ZnSe secondary phases are taken into consideration. The optical functions for ZnSe and Mo were inserted into the model from the database of the WVASE software; $MoSe_2$ was taken from our previous investigation [14]. The optical function of CZTSe was then extracted by the described fitting procedure. Our applied model includes (top to bottom) an EMA surface roughness layer (Bruggeman effective medium approximation [13]) with a 50:50 void:top layer mixture, an EMA ZnSe:CZTSe layer with a variable fraction, the actual CZTSe absorber, a standard intermix layer for modeling the non-ideal interface (EMA with 50:50 mixture of neighboring phases), a ZnSe layer, another standard intermix layer, a $MoSe_2$ layer, another standard intermix layer, and the Mo substrate. The intermix layers were set to a constant value and are not included as fitting parameters. We found that a thickness of only 1nm is already sufficient to account for the non-ideal interface between neighboring layers. Further reduction or the total absence of these layers lead to significantly worse fitting results. Furthermore, we find that these layers strongly reduce the correlation between neighboring layers and are essential for achieving unique fitting results. The structure of the optical model is illustrated in Fig. 1.

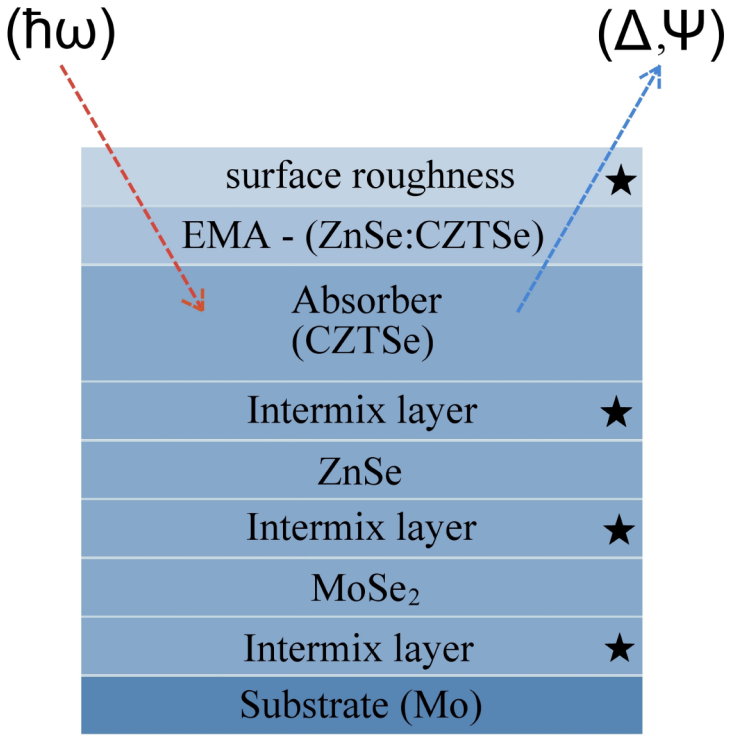

Fig. 1. Schematic representation of the multi-layer optical model for SE data analysis. Layers labeled with a star are based on Bruggeman Effective Medium Approximation (EMA), with a 50:50 mixture of adjacent layers. The ZnSe: CZTSe EMA layer contains a variable fraction which is varied in the fitting procedure.

Optics EXPRESS

Figure 2 shows experimental Ψ and Δ data for each sample together with the fitted curves from the modelling. For better viewing only the results for the 70° angle is shown. SE data for the energy range between 410 nm-1700 nm (3.0 eV and 0.75 eV) was used for all samples in the fitting procedure. Data points below 410 nm (above 3.0 eV) were not considered for the fit, due to high signal noise. This occurrence of noise was observed for many polycrystalline CZTSe thin film samples. The origin of the noise could not be identified with certainty, but it might originate from inhomogeneities, surface roughness and/or other artefacts at the front side of the sample such as intermixing of small amounts of further secondary phases.

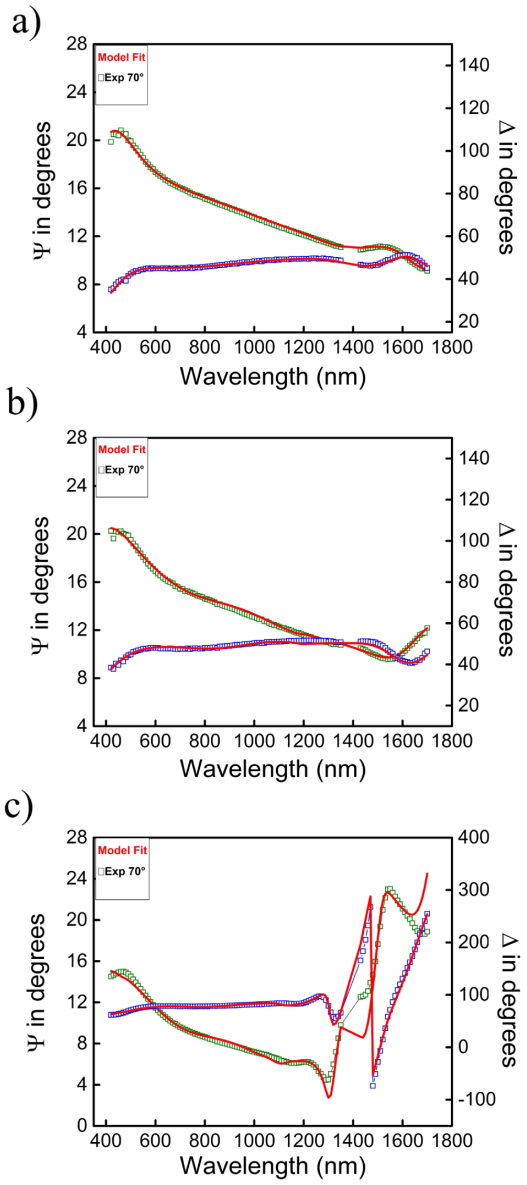

Fig. 2. Measured and fitted ellipsometry data for samples A, B, and C, respectively. Psi (Ψ, green colored symbol) and Delta (Δ, blue colored symbol) values are shown for only one incidence angle (70°) together with the fit results (red solid lines)

Optics EXPRESS

The thicknesses of layers extracted from the fitting procedure along with their standard deviations are presented in Table 1 for each sample. All samples show a thickness of the surface roughness layer which is in the usual range for SE evaluations. However, the value for sample B appears very low. Note, the fitted numbers for the surface roughness usually do not reflect the real surface roughness values of the sample. They may rather give an indirect indication for the actual roughness of the surface. The fitted numbers are influenced further by the morphology/shape of the grains, lateral inhomogeneities of the optical function and of the roughness itself. Nevertheless, the extracted thicknesses for the absorbers and the $MoSe_2$ layer for sample C are supported by SEM results, as shown in Table 1.

According to fitting results, each sample has ZnSe and $MoSe_2$ secondary phases on the back side of the absorber, with different amounts, showing by far the highest MoSe2 amount for sample C. Further, only Sample C shows ZnSe fractions on the front side of the absorber. The different amounts of $MoSe_2$ and the ZnSe:CZTSe mixture on the front side of sample C can be explained by the different processing routine for sample C compared to samples A and B, and will be discussed further below. The mean square error (MSE) which shows the fit quality indicates a very good fit for samples A and B, whereas the MSE for sample C is significantly larger. This can be explained by a higher degree of inhomogeneities and worse crystal quality of the absorber due to the distribution of ZnSe secondary phases, or higher disorder in the crystal for the case of sample C, compared to sample A and B. In fact, scanning electron microscope (SEM) pictures from samples A and B show ZnSe inclusions at the backside of the CZTSe film (not shown here). In contrast to this, sample C does not show any ZnSe inclusions but may rather contain a network of ZnSe nanodomains which percolate the entire CZTSe film. An earlier investigation on samples prepared by the same procedure as sample C revealed this network of ZnSe nanodomains by atom probe tomography [20]. A network of two phases as described is hard to model by this approach. The modeling of such a network would be possible with a strongly modified model which includes a Maxwell-Garnett EMA instead of the widely used Bruggeman EMA [21,22]. We do not follow this approach due to its higher complexity and because it does not reflect a general optical model for the whole set of samples. This deficit of the presented optical model for sample C can additionally lead to a worse MSE in the fitting procedure for the SE data as described above. Nevertheless, we can still state that this model is at least sufficient to determine the presence of ZnSe secondary phases for each sample.

Thickness values extracted from SEM measurements (see Table 1) confirm the thicknesses from SE for the absorber and for the $MoSe_2$ layer (sample C). Further, the presence of ZnSe secondary phases is confirmed by SEM (sample A and B) and by APT (sample C), as described above, respectively.

Optics EXPRESS

Table 1. Fitting results of the optical model including the thicknesses and their standard deviations are shown for surface roughness, EMA layer with the ratio of components, CZTSe absorber layer, the interface layer. Mean Square Error (MSE) from SE, and the thicknesses of absorbers $MoSe_2$ layers from SEM.

Energy fit range 0.75-3.0 (eV)	Roughness (nm)	EMA layers (nm)	CZTSe (nm)	Interface layer (nm)		MSE	SEM results (nm)	
		(ZnSe: CZTSe)		**ZnSe**	**$MoSe_2$**		**CZTSe**	**$MoSe_2$**
Sample A	14.0±0.1	**8.11**±6.8 (0.0:100) ±6.3	1086±8.7	**4.0**±3.5	**4.0**±3.9	1.7	1150 ±150	≈0.0
Sample B	2.3±0.2	**9.5**±5.0 (0.5:99.5) ±2.1	1033±18	**26**±15	**26**±13	3.1	950 ±150	≈0.0
Sample C	12.0±0.5	**9.2**±1.6 (40:60) ±6.6	1242±43	**18**± 13	**236**±4.6	26.4	1200 ±100	185±50

3.1.1 Band gap calculation

To calculate the band gap of CZTSe thin films, the refractive index and extinction coefficient were extracted from the SE results. The optical absorption coefficient "α" of CZTSe can be calculated by the expression of $a = \frac{4\pi k}{\lambda}$ where k is the extinction coefficient, and λ is wavelength. Additional to this, we calculate the absorption coefficient by optical reflection and transmission measurements by using the formula $a = -\frac{1}{t}\ln\frac{T}{(1-R)^2}$ where "t" is the film thickness (determined by SE fitting results and SEM), R and T are reflectance and transmittance, respectively.

The relationship between absorption coefficient and photon energy for a direct semiconductor is [23]:

$$a = \frac{A(hv - Eg)^{1/2}}{hv} \quad (1)$$

Where A is constant, hν is the photon energy, Eg is the band gap. Optical band gap can be calculated by extrapolating the linear region of $(\alpha h\nu)^2$ versus hν. In Fig. 3 a) and b), we show the extraction of the band gap by this approach for SE and R&T results, respectively. The found band gap values from SE measurements amount to 0.99 ± 0.02 eV for sample A and 0.97 ± 0.01 eV for sample B. Surprisingly the behavior of sample C shows two possible transitions at 0.93 ± 0.01 and 1.020 ± 0.001 eV. We explain this behavior by the discussed fact that sample C does not contain a single phase kesterite bulk, but rather a network of CZTSe and a ZnSe secondary phase. Due to a superposition of the signal response of these two phases which, as discussed above, cannot be resolved by our model, the extracted absorption coefficient may include artefacts. Due to this restriction of our approach we are not able to distinguish such an artefact caused by the discussed network structure from a further transition in CZTSe, e.g. caused by second band gap or regions with different band gap [5,20]. Nevertheless the photon energies of the observed transitions are in the range of reported band gap values [24–27]. Note, the extracted absorption values for sample C are

Optics EXPRESS

lower than for the other two samples. Therefore, a multiplication factor of 4 is operated for sample C.

The evaluation of the R&T measurements gives band gap results of 0.99 ± 0.02 eV, 0.94 ± 0.01 eV and 0.99 ± 0.01 eV for sample A, sample B, and sample C, respectively. The differences in band gap values between samples can be explained by different order-disorder ratios and different compositions [28]. Furthermore, the existence of secondary phases may lead to distortions of the extracted absorption spectra due to superpositioning of optical transitions of different phases [29]. However, band gap results are similar for both techniques. The slight discrepancy in the results for both methods can be explained by their different sensitivities for bulk and surface. R&T is a bulk sensitive method, giving equal weight to all parts of the entire layer. For SE we can expect a higher influence of the surface region (depending on layer thickness, probing wavelength and absorption coefficient). Due to the ambiguity of the fitting regions for the linear extrapolation the extracted values contain a systematic error. The given error was determined from extrapolations for varied fitting regions for each spectrum.

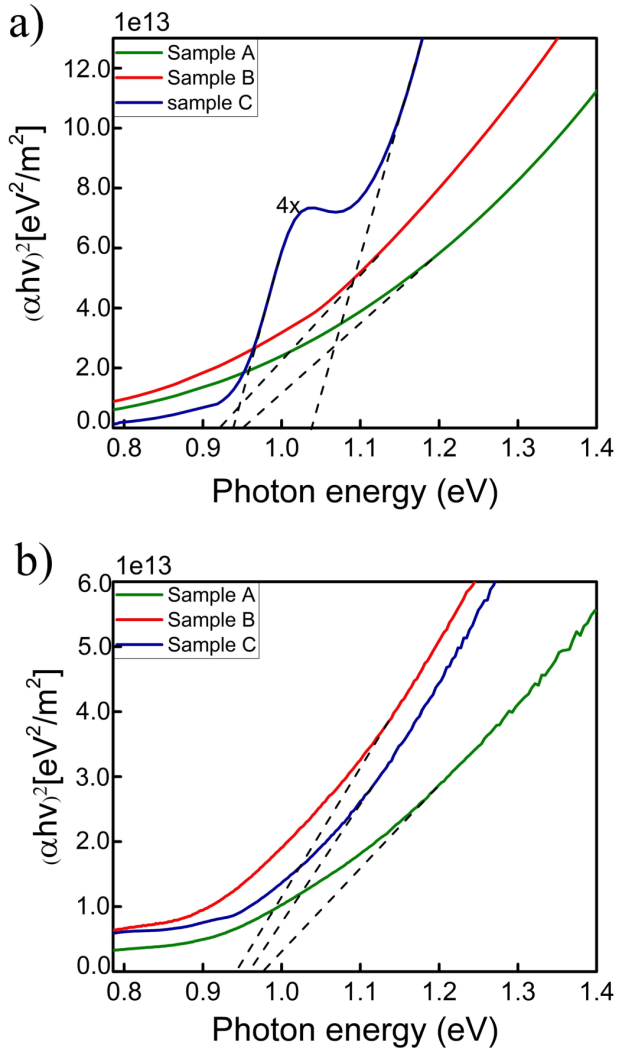

Fig. 3. The plot of $(\alpha h\nu)^2$ vs. hν from a) SE results b) R&T results for all samples and extraction of band gaps via linear extrapolation to zero (dashed lines).

Optics EXPRESS

3.2 Raman results

Raman spectroscopy was performed on the front and back side of absorbers and the SLG/Mo substrate after lift-off process for each sample at 532 nm and 457.9 nm excitation wavelengths. The reason for using a second excitation wavelength is to identify small amounts of ZnSe in the absorber. To represent a large area of the samples, the average of four different areas is shown in Fig. 4. The Raman signal from ZnSe secondary phases in CZTSe is strongly enhanced due to the resonant Raman effect for the 457.9nm laser, as the energy of its photons is in the region of the band gap energy of ZnSe (~2.7 eV). Hence, even very small ZnSe fractions in the sample can be identified with the "blue" excitation laser [10,30]. The utilization of solely the 532 nm excitation can only reveal very large amounts of ZnSe in the sample. Therefore, "green" excitation is not sufficient to reliably detect ZnSe secondary phases in CZTSe samples.

The Raman results for the 532nm excitation show the expected CZTSe fingerprints for the front side of the absorbers (Fig. 4a) without any indications for secondary phases. However, at 457.9 nm laser excitation, sample C shows additionally a ZnSe peak at 250 cm^{-1}, whereas a clear CZTSe fingerprint without indication for any secondary phases is confirmed for samples A and B. These results are in agreement with the SE results as discussed before in Section 3.1, i.e.: no indication for ZnSe at the front side of sample A and sample B neither by SE nor by SEM. and co-existence of ZnSe with CZTSe at the front side of sample C. Furthermore, as discussed above a reported APT study on similar samples shows the existence of a ZnSe network in the entire absorber [20].

At 532 nm excitation wavelength, the Raman measurements on the back side of the absorbers (Fig. 4b) show clear CZTSe fingerprints without any indication of secondary phases. However, at 457.9 nm excitation wavelength, all three samples show a clear ZnSe peak at 250 cm^{-1} which is in accordance with SE results (see Table 1).

The Raman modes for CZTSe are still visible in all samples for 457.9 nm, however with very low intensities for samples A and B, at which the second main peak around 175 cm^{-1} is hardly visible. In contrast, both main CZTSe peaks are still fairly distinguishable for sample C. This different behavior of samples can be explained by the different growing process which leads to a different distribution of ZnSe secondary phases as discussed in Section 3.1. ZnSe secondary phase in sample C is distributed as a network in entire bulk. Therefore, a clear appearance of peaks for both phases CZTSe and ZnSe is expected. In contrast, sample A and sample B contain ZnSe inclusions at the back side of the absorber, which may hamper the detection of CZTSe for sample A and sample B, resulting in the very low intensity of CZTSe peaks.

Raman spectra for the remaining substrate (Fig. 4c) show $MoSe_2$ peaks for all three samples. However, the $MoSe_2$ peak intensities of sample A and sample B are much lower than the $MoSe_2$ intensity of sample C. Therefore; these two spectra were multiplied by a factor of 5 for better viewing. Raman spectroscopy results are in good agreement with SE results, which show by far the highest thickness (amount) of the $MoSe_2$ secondary phase for sample C (see Table 1).

Optics EXPRESS

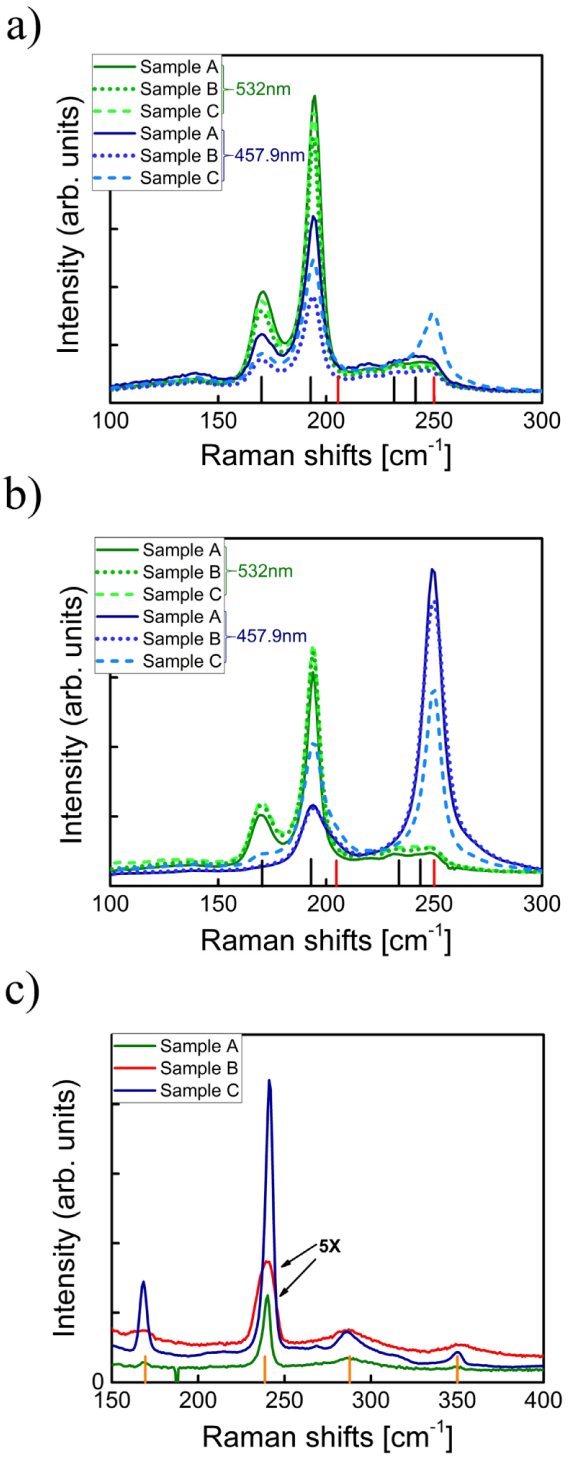

Fig. 4. Raman spectra for each sample (a) front side of the samples, (b)back side of samples and (c) the remaining substrate after lift-off process. Excitation wavelengths are indicated in a) and b) by green and blue lines for 532nm and 457.9 nm, respectively. In figures a) and b) the black and red markers show the peak positions of CZTSe and ZnSe phases. In figure c) orange markers show $MoSe_2$ peaks.

Optics EXPRESS

3.3 Photoluminescence results

PL spectroscopy was performed on the front and back side of the absorbers with different excitation wavelengths. The aim of using different excitation wavelengths was to distinguish between optical transitions of the absorber and present secondary phases. PL spectra can also be used to determine the band gap of a semiconductor if the material has no tailing and the emission is dominated by band to band transition. However, it is not the case for CZTSe and the main PL peak is usually observed around 100 to 150 meV below the band gap energy due to tailing and the contribution of defects [31,32].

In Fig. 5, we show the PL spectra for each sample. Note, that the plotted spectra show the averaged result from two different areas to represent a large area of the sample. The maximum PL position of the main peak from the kesterite occurs for all samples in the range 0.83-0.86 eV, with no correlation to the discussed band gaps of the samples. The slight differences between the PL peak positions can occur due to different compositions, which may lead to different tailing properties and other dominating defects. The PL spectra from the backside of each absorber show additionally a broad peak at around 1.2 eV, known as a ZnSe defect transition in literature [30,33–35]. These results are in good agreement with SE and Raman results: All samples show clear evidence for the existence of ZnSe secondary phases at the back side of the absorber for both SE and Raman spectroscopy (see Table 1 and Section 3.2).

The intensity of the ZnSe defect transition peak depends on the applied excitation wavelength: with increasing excitation wavelength, the intensity of this defect transition diminishes. This demonstrates that the defect transition can be probed selectively by the choice of the wavelength. Sufficiently short wavelengths (higher photon energies) are necessary to excite the involved defect states. Further, by choosing long wavelengths, the ZnSe defect transition can be excluded from the spectrum to allow for measuring only the PL from CZTSe. This clean-up procedure is necessary for more complex evaluations of the high energy wing of the CZTSe PL for e.g. extraction of quasi-Fermi level splitting by Planck's generalized law [36–38].

For the front side of the absorbers, only the measurement with the shortest excitation wavelength (532 nm) is shown in Fig. 5, since no differences between the results from different excitation wavelengths could be observed (not shown here). The PL maxima for the front side match the peak positions found on the back surfaces. Further, none of the PL spectra shows any contribution from ZnSe. This is in accordance with SE and Raman results for samples A and B. However, both SE and Raman results show clear indications for ZnSe at the front side of sample C. This discrepancy can be interpreted as an indication of a higher sensitivity of SE and Raman spectroscopy for the detection of small fractions of ZnSe secondary phase in CZTSe samples.

Optics EXPRESS

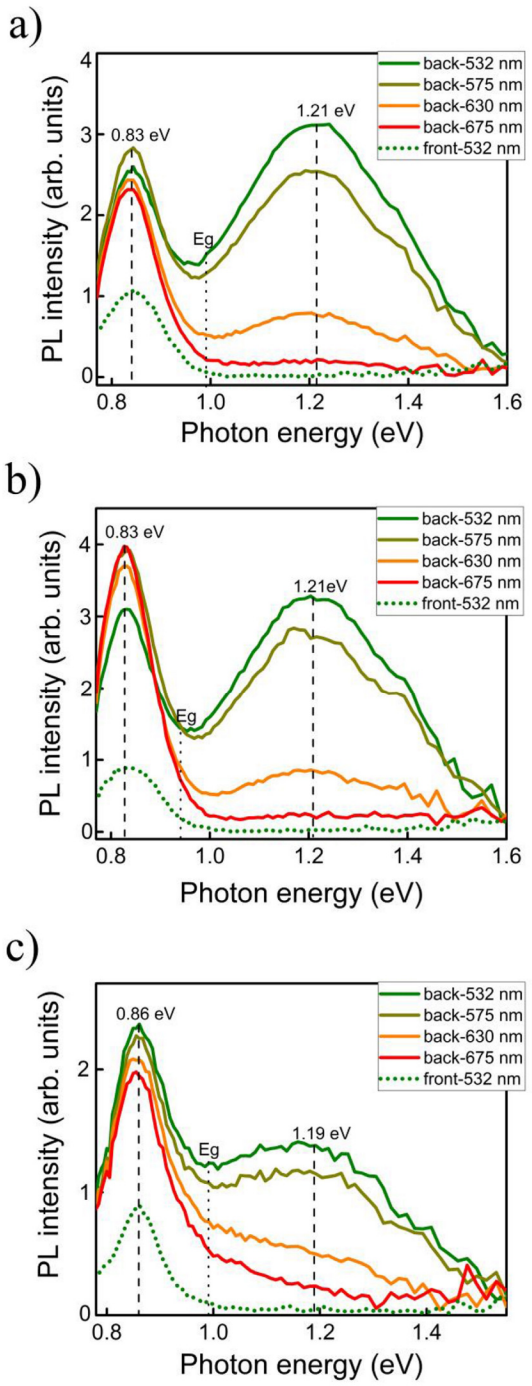

Fig. 5. PL spectra for a) sample A, b) sample B, c) sample C, respectively. Solid lines represent the backside of each absorber for different excitation wavelengths, these are given in the legend and are color coded, respectively. Dotted lines represent the front side of the absorbers for only 532 nm excitation. The band gap from R&T measurements is indicated in the plot.

Optics EXPRESS

4. Conclusions

In this paper, we have demonstrated that SE can be used as a non-destructive technique to detect secondary phases within a layer and/or at the back side of the absorber (SLG/Mo/CZTSe). The existence of $MoSe_2$ at the back side and its amount can be determined by SE. Additional to this, the presence of ZnSe at the front and back side of the absorber can be determined by SE. The results are confirmed by Raman and PL spectroscopy.

We use a complex optical model based on a multi-layer approach for evaluation of SE data. The construction of an optical model which also contains all minor constituents in the sample, such as fractions of secondary phases, is critical to making accurate interpretations on the properties of the material. If this requirement is met, SE allows for accurate extraction of optical parameters such as band gap, refractive index, and extinction coefficient. The results show that band gap determination by SE is as reliable as R&T measurement, and works on CZTSe on Mo substrates in advantage over R&T. The slight discrepancy of results extracted from both techniques is due to the different sensitivities for bulk and surface.

We also observe that the intensity of the ZnSe defect transition peak in PL shows a dependency on the applied excitation wavelength. Therefore, it is important to select the wavelength adequately for selective excitation or removal of the ZnSe defect transition in the measured PL spectra.

Acknowledgments

The work at the LCP research group (Oldenburg) is funded by EWE AG, Oldenburg, Germany, and the BMBF (German Ministry of Education and Science), funding Nr. 03SF0530A (project “Free-Inca”). The work at the LPV group (Luxembourg) was supported by Fond National de la Recherche (FNR) under project KITS2 (Grant No. C11/MS/1202439).